Article

Experimental Study on Electric Potential Response Characteristics of Gas-Bearing Coal During Deformation and Fracturing Process

Zhonghui Li [1,2,3,4,†,*], **Yue Niu** [1,2,3,4,†], **Enyuan Wang** [1,2,3,4,*], **Lanbo Liu** [5], **Honghao Wang** [6], **Mingfu Wang** [7] **and Muhammad Ali** [4,8]

[1] Key Laboratory of Gas and Fire Control for Coal Mines (China University of Mining and Technology), Ministry of Education, Xuzhou 221116, China; ahsyls69@cumt.edu.cn

[2] Engineering Research Center for Coal Gas Control, China University of Mining and Technology, Xuzhou 221116, China

[3] State Key Laboratory of Coal Resources and Safe Mining, China University of Mining and Technology, Xuzhou 221116, China

[4] School of Safety Engineering, China University of Mining and Technology, Xuzhou 221116, China; muhammad.ali@cumt.edu.cn

[5] Department of Civil & Environmental Engineering, University of Connecticut, Storrs, CT 06268, USA; lanbo_liuuconn@163.com

[6] Yanghe Coal Industry Limited Company, Zhengzhou Coal Industry (Group), Zhengzhou 452382, China; whh19901110@163.com

[7] Xinzheng Coal Power Limited Company, Zhengzhou 450000, China; yuer_new@126.com

[8] Department of Mining Engineering, Balochistan University of Information Technology, Engineering and Management Sciences, Quetta 87300, Pakistan

* Correspondence: lzhemr@126.com (Z.L.); weytop@cumt.edu.cn (E.W.); Tel.: +86-13814443973 (Z.L.); +86-15150037723 (E.W.)

† These authors contributed equally to this work.

check for updates

Abstract: Coal mass is deformed and fractured under stress to generate electrical potential (EP) signals. The mechanical properties of coal change with the adsorption of gas. To investigate the EP response characteristics of gas-bearing coal during deformation and fracture, a test system to monitor multi-parameters of gas-bearing coal under load was designed. The results showed that abundant EP signals were generated during the loading process and the EP response corresponded well with the stress change and crack expansion, and validated this with the results from acoustic emission (AE) and high-speed photography. The higher stress level and the greater the sudden stress change led to the greater EP abnormal response. With the increase of gas pressure, the confining action and erosion effect are promoted, causing the damage evolution impacted and failure characteristics changes. As a result, the EP response is similar while the characteristics were promoted. The EP response was generated due to the charge separation caused by the friction effect etc. during the damage and deformation of the coal. Furthermore, the main factors of the EP response were different under diverse loading stages. The presence of gas promoted the EP effect. When the failure of the coal occurred, EP value rapidly rose to a maximum, which could be considered as an anomalous characteristic for monitoring the stability and revealing failure of gas-bearing coal. The research results are beneficial for further investigating the damage-evolution process of gas-bearing coal.

Keywords: gas-bearing coal; electrical potential; charge separation; gas adsorption; damage evolution

1. Introduction

As the basic energy used in the world, coal resources play an important part in industrial production and economic life [1]. During mining activities, coal and gas outburst disasters greatly threaten safe production in coal mines, leading to serious casualties and property loss. Examples of accidents include coal and gas outburst and rock burst [2–4]. For example, in 2014, a coal burst damaged mine equipment seriously and resulted in the death of two miners in the Austar coal mine in Australia [5]. Therefore, the research on revealing the initiation and generation mechanism of coal and gas outburst disasters is of great significance for monitoring the stability of coal-rock mass while mining, and predicting the generation of coal and gas outburst disaster [6].

Under the combined effect of ground stress, mining-induced stress, and gas pressure, the internal damage of coal-rock mass constantly changes to finally trigger structural instability and dynamic failure, which causes the coal and gas outburst disaster [7]. Monitoring the stress state and damage-evolution process of coal-rock mass is the key to monitoring and early-warning of coal and rock outburst disasters [8]. At present, with the gradual reduction of coal resources in the shallow underground coal seams, coal mining shifts to deep underground coal seams [9]. Deep coal seams basically contain abundant high-pressure gas and the coupling effect of stress and gas gradually imposes increasing influences on the state of the coal mass [10]. When the gas is sufficiently adsorbed by the coal, the gas is stored in the pores of the coal mass at adsorbed state and free state to form gas-solid coupling system with the coal mass [11]. The formation of this gas-solid coupling system changes the physical and mechanical properties of the coal (including mechanical property, deformation and fracture process, and failure mode). The formation of the system further influences the occurrence of various disasters, such as coal and gas outburst and rock burst [12].

Energies are released during the initiation and occurrence process of coal and gas outburst disasters. The released forms include the elastic energy, acoustic energy, electromagnetic energy, etc. [13]. Therefore, numerous geophysical methods (such as acoustic emission (AE) and electromagnetic radiation) are developed to monitor the stability and predict the failure of the coal mass [14,15]. The methods have been widely explored in the laboratory, and corresponding technologies also have been applied in mining activities in the field [16–20]. Previous studies indicated that coal-rock mass could be electrically charged during deformation under load. It triggers the electrical potential (EP) response on the material surface. The EP response is closely related to the deformation and fracture of the coal mass, which characterizes the stress state and damage-evolution process of the coal mass. The abnormal change of the EP can be considered as the precursor of failure of coal-rock materials. Yoshida [21] found that the EP changed markedly just prior to dynamic rupture. Takeuchi et al. [22,23] studied the electrokinetic properties of quartz and granite and demonstrated that the fracture surface and sliding friction surface were charged with the density up to 10^{-4}~10^{-2} C/m^2. By exploring the EP effect of the coal-rock not containing gas under load, Wang et al. [24] showed that the change of the EP was highly correlated with loads and rates of load change. The distribution of the EP field corresponded well to that of strain field. Additionally, they discussed different mechanisms of the EP response by referring to the electromagnetic radiation (EMR) [25]. Archer et al. [14] found EP signals were stimulated during linear-elastic and -inelastic deformation, which was associated with micro-cracking. As a conclusion, the article provided an effective and advanced method for structural health monitoring of rocks. Niu et al. [26] presented the EP response characteristics and its mechanism in a similar simulation of coal-mining activities. The above research provides a favorable theoretical basis for monitoring the failure of coal-rock mass by testing the EP response [27–29].

Previous research on the EP effect of the coal-rock mass was mostly carried out on the coal-rock mass not containing gas. However, research on the EP response characteristics of coal dynamic failure under the stress-gas coupling effect and the influence of gas is rare. To solve the problem, the influences of the stress-gas coupling effect on the deformation and fracturing process of the coal mass were investigated. Furthermore, a multi-parameter test system for gas-bearing coal under load was designed to carry out compressive tests under different gas pressures. During the loading process,

the various responses (including EP and AE) during the deformation process of gas-bearing coal under load were synchronously recorded. Simultaneously, the evolution process of coal fractures is subjected to high-speed photography in real time by using an industrial camera. The AE count can reflect the micro-fracturing happening during the damage and deformation of the coal mass while the amplitude of the signals can reflect the intensity of micro-cracks [30]. The high-speed photography can catch the instantaneous state of crack evolution of the coal mass during different loading stages [31]. This method allows us to analyze the EP response and the damage evolution of the coal mass. Therefore, the research result is beneficial to further reveal the initiation mechanism of coal-rock dynamic disasters. In this way, the attempt is carried out to provide valuable information about the damage evolution under the stress-gas coupling effect and monitor the failure of the coal mass by using the EP response.

2. Experimental Materials and Methods

2.1. Specimen System

The experiment was conducted in the Faraday shielded room in China University of Mining and Technology. It could effectively prevent the electric noise from affecting the recorded signals [15]. The experimental system was designed and established individually to acquire multiple types of information during loading process of the gas-bearing coal (see Figure 1). The subsystem parts are shown as follows.
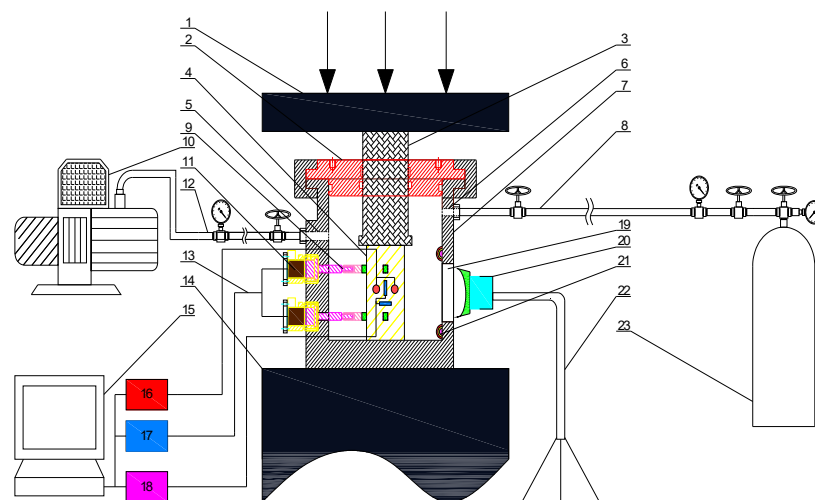

Figure 1. Experimental system of multi-data acquisition during loading process of gas-bearing coal.

Number of parts in experimental system of Figure 1.

1	loading plate	13	data transmission line
2	chamber cover	14	supporting base
3	loading shaft	15	data acquisition control host
4	specimen	16	EP controller
5	exhausting hole	17	AE controller
6	inflating hole	18	loading controller
7	chamber	19	visible window
8	gas transmission line	20	industrial camera
9	waveguide rod	21	illumination source
10	vacuum pump	22	triangular bracket
11	AE sensor	23	gas cylinder
12	exhaust line		

It includes a hermetically sealed chamber subsystem, an axial compressive loading subsystem, an EP monitoring subsystem, an AE monitoring subsystem, a high-speed camera shooting subsystem, and a gas inflating-extracting subsystem

(1) The hermetically sealed chamber subsystem, including a chamber cover, a loading shaft, gas spiracles, waveguide rods, and a visible window (see Figure 1). The gas can be pumped into the chamber with spiracles and kept at a certain pressure after closing the valve.

(2) The EP monitoring subsystem, including the electrode, data transmission line, an amplifier, A/D converter and data storage. When the EP signals were measured by the electrode on the surface of specimen, and then translated by the data transmission line. The host computer can analyze the signal and display it in real time. The maximum sampling frequency is 100 kHz.

(3) The AE monitoring subsystem, reaching a series of functions, such as the parameter setting, signal acquisition, data storage, graphics display, waveform acquisition, and spectral analysis. During the loading process of the specimen, it can acquire simultaneously the counts and energy of AE signals and locate the damage position inside the specimen.

Conventional AE sensors fail to endure high gas pressure. However, in previous monitoring methods, sensors are distributed on the surface of gas-bearing containers, which causes loss and inaccurate measurements of AE signals [32]. To solve the problem, the specialized waveguide rods are designed, as shown in Figure 2. The one end of the waveguide rods is connected to the specimen while the other end is connected to the AE sensor. Moreover, coupling agents favorable for conduction of acoustic waves are uniformly painted on the two ends of the waveguide rods. Composite materials are filled between the waveguide rods and the wall of the gas cylinder, to prevent the transmission of acoustic waves from waveguide rods to the gas cylinder. In this way, AE signals generated by the specimen can be completely transmitted to the AE sensors through waveguide rods as far as possible. The composite materials are connected to the waveguide rods through the screw joints so that the waveguide rods can move to the wall of the cylinder relatively and the specimen can be readily dismantled. Besides, the space between the waveguide rods and the composite materials is sealed through a flexible seal ring. It is an innovative design to transmit the AE signals of coal fracture in the high-gas environment through the waveguide rods.
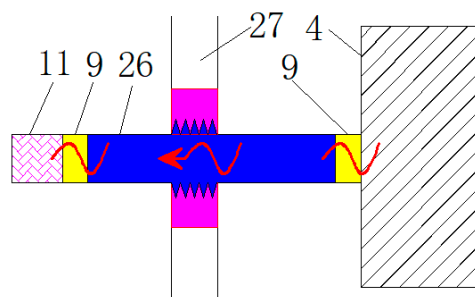

Figure 2. Schematic diagram of AE signal from waveguide wave. 11—AE sensor; 9—coupling agent; 26—waveguide rod; 27—chamber wall; 4—specimen.

(4) The axial compressive loading subsystem, including a loading frame, a hydraulic drive device, a controller host, and a program (see Figure 3). It can record the data of displacement, load, and time synchronously during the loading process. The oil source is placed outside the faraday shielded room, to reduce the interferon on the experiment.

Figure 3. Axial compressive loading subsystem. (**a**) Loading frame. (**b**) Hydraulic drive device and controller host.

(5) The high-speed camera shooting subsystem. It includes the industrial camera, the illumination source, and the triangular bracket. The instant crack expansion on the specimen surface during loading process can be shot clearly by using the industrial camera through a visible window. The resolution ratio of photograph is up to 1920 × 1080 pixels with 40 frames per second.

(6) The gas inflating-extracting subsystem, including the vacuum pump, gas transmission, exhaust lines, and gas cylinder. The gas also can be inflated into the chamber by the gas transmission line and extracted after the experiment.

Under the coupled action of loading stress and gas pressure, the system could be used to conduct the compression experiment of coal. During the process, the signals of EP and AE and crack photograph could be obtained in real time to be analyzed.

2.2. Specimen Preparation

The coal mass was derived from No. 5 coal seam in Yangzhuang coal mine, Huaibei City, China. Then the specimens were prepared according to the standard size of 50 (width) × 50 (height) × 100 (length) mm (see Figure 4).

Figure 4. Coal specimen. With size of 50 (width) × 50 (height) × 100 (length) mm.

2.3. Experimental Scheme

The experiment was carried out according to the following steps.

(1) First, all specimens were placed in the sealed dry container for 24 h before the experiment, to prevent them from absorbing excessive water.

(2) The airtightness of the cylinder was tested to ensure that the cylinder has a favorable sealing effect. The various parts of the test system were connected and kept a turn-on state.

(3) Electrode and waveguide rods (the other end connected to AE detectors) were distributed on the surface of the coal mass and sealed in the cylinder. By using a vacuum pump, the cylinder was vacuumized. To provide electrical isolation, two thin teflon-plates were placed on the top and bottom of specimen.

(4) Gas was injected into the cylinder. After reaching a certain pressure, the pressure was stabilized for 8 h so that the coal mass could fully adsorb gas.

(5) Experimental parameters were set.

(6) The load was applied on the specimen by using the press to further synchronously measure various data such as EP and AE.

(7) After the specimen was damaged, the experiment was ended and gas in the gas cylinder was released.

3. Experimental Results and Analyses

3.1. Test Results of Multi-parameters during the Damage of Gas-Bearing Coal under Load

In the series, experiments under different gas pressures were carried out. As the example, the experimental results under 2.0 MPa were analyzed as follows. The experimental parameters were set as Table 1.

Table 1. Setting of experimental parameters.

Shielding Effect for Electromagnetic Signal	Threshold Value for AE Signal Acquisition	Axial Loading Rate of the Press	Gas Pressure in Chamber
85 dB	45 dB	50 N/s	2 MPa

(1) Responses of strain and stress

During loading process, the gas pressure was kept at 2 MPa after reaching adsorption equilibrium. The loading stress on the top surface of specimen by loading system is defined as loading stress (LS). Owing to gas pressure, the initial LS was not zero. The curves of stress and strain with respect to loading time are shown in Figure 5.
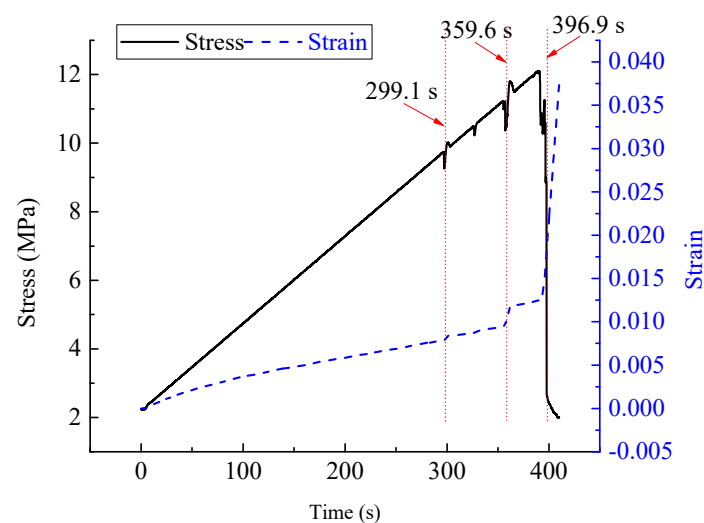

Figure 5. Curves of stress and stain with respect to loading time. The red dotted lines indicate the mutation time of curves.

It can be seen from Figure 5 that with increasing loading time, the stress and strain on the specimen gradually rose. Stress and strain suddenly changed at small amplitudes both at 299.1 s and 359.6 s, implying that the great damage appeared in the local zone of the specimen. Moreover, the local crack expansion resulted in the instant increase of the specimen deformation while stress fluctuated. With the constant loading, stress and strain constantly rose. At 396.9 s, the primary crack was found and therefore the structure of the specimen lost stable. In this case, stress dramatically and suddenly changed and rapidly reduced while strain rapidly increased.

(2) Responses of AE signals

Previous research shows that under the effect of external load, the coal mass is damaged to thus lead to the initiation and expansion of cracks, consequently triggering numerous AE events [30]. Dislocation and slippage between particles in coal matrix can also induce the fracturing of bridge bonds between coal molecules, consequently generating AE phenomenon [33]. AE counts characterize the times of micro-cracking happening during damage and fracturing of the coal mass while the amplitude of the signals reflects the strength of micro-cracking. The parameters related to AE can be used to describe the evolution process of damage and crack expansion and release process of energies in the coal mass, to further judge the deformation and fracturing of the coal specimen and predict the occurrence of failure of the coal specimen [20]. Figure 6 shows the curves of AE counts and MAS (mean amplitude strength) with respect to loading time under gas pressure of 2 MPa.
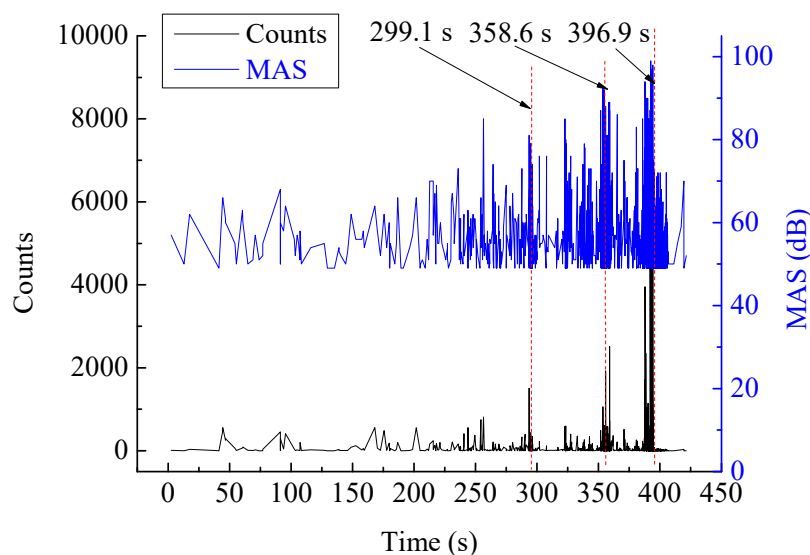

Figure 6. Curves of AE counts and MAS with respect to loading time.

As shown in Figure 6, in the early stage of loading, there were few AE signals with low AE count and amplitude. AE signals were mainly generated due to the mutual slippage of primary cracks in compacted gas-bearing coal and the friction between particles. With the constant growth of stress, the coal damage was constantly aggravated, gradually transiting to plastic damage stage from elastic stage. In the process, new cracks initiated, split, and expanded along the weak structural plane to generate new fracturing signals thus further. Therefore, the AE counts and amplitude both increased during which the amplitude became more concentrated. At 299.1 s and 358.6 s, the specimen was greatly damaged and therefore cracks rapidly expanded, resulting in many fracturing events. In this context, fractured zones were formed in local areas and high-energy gas constantly impacted the coal mass along the weak structural plane, also exhibiting a significant friction effect. AE counts rose in an impulse type, with a high amplitude, reflecting the sudden increase in micro-cracks in the coal mass and the large crack strength, thus releasing huge elastic energies. The result confirmed to the phenomenon that stresses suddenly changed at corresponding time moment in Figure 5, which can be taken as a favorable complementary evidence. When the primary cracks occurred at 396.9 s, AE count

and amplitude both reached the maximum. It indicated that the number and strength of micro-cracks in the coal mass dramatically rose to thus result in the great expansion and cut-through of cracks, consequently triggering the failure of the specimen. After the primary crack was found, AE signals rapidly reduced and almost disappeared.

(3) Responses of crack expansion

The evolution processes of crack expansion at different time moments were recorded by applying high-speed photography, as shown in Figure 7.
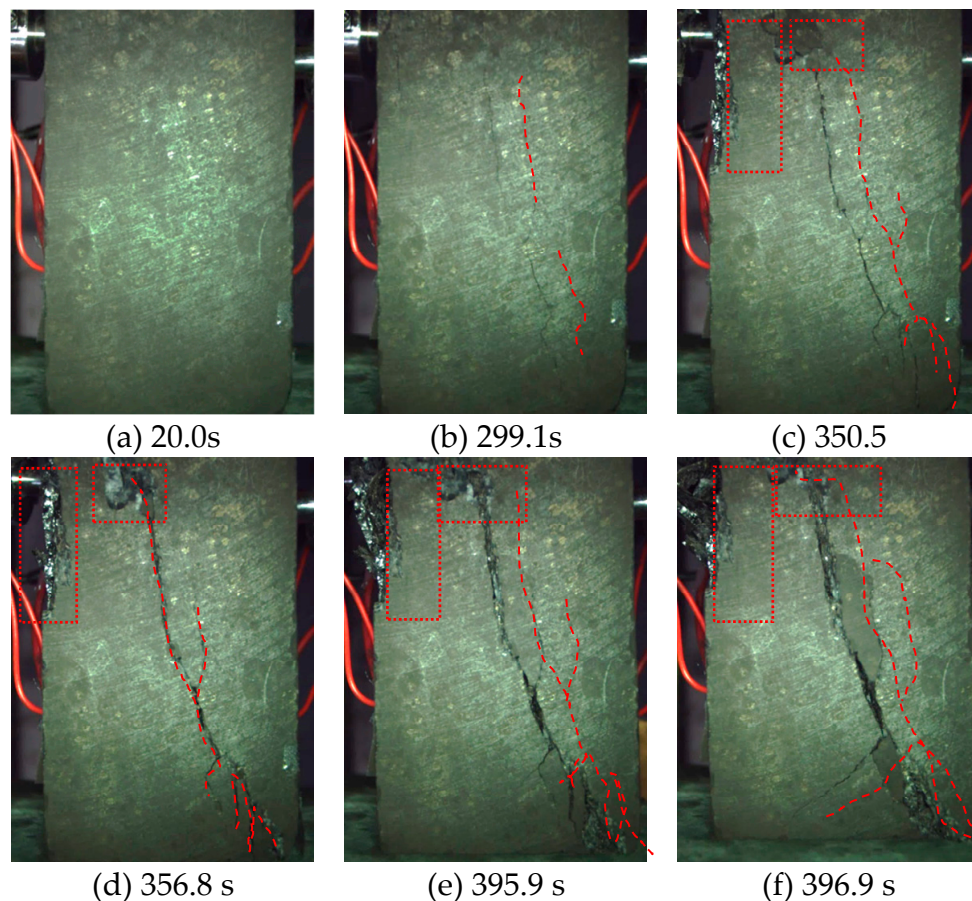

| (a) 20.0s | (b) 299.1s | (c) 350.5 |
| (d) 356.8 s | (e) 395.9 s | (f) 396.9 s |

Figure 7. Pictures of fracture expansion in gas-bearing coal under load at different time moments; red imaginary lines refer to the tracks of crack expansion while red wireframes denote the centralized zone with cracks of specimen.

As shown in Figure 7, in the early stage of loading (for example, at 20.0 s), although accumulated damage of the specimen was present, it was insignificant, and no micro-crack was formed on the surface of the specimen. With increasing stress, the micro-defects and micro-cracks in the coal-rock mass gradually aggregated and connected in local zones after undergoing constant extension and expansion in the early stage, showing certain self-organization, thus triggering the generation of micro-cracks in the coal-rock mass. At 299.1 s, stress suddenly changed at a small amplitude and therefore two separated thin and long micro-cracks were formed on the surface of the specimen. At 350.5 s, the damage and fracturing of the coal mass aggravated and two previous micro-cracks mutually cut through and further expanded to thus form multiple secondary cracks. Additionally, microscopic breakage appeared at the left side of the specimen and the top inclined to the left. At 356.8 s, the stress approximated to the maximum, and the width and length of the primary cracks further rose, and the number of secondary cracks increased and constantly expanded. The damage zones at the left side and the top of the specimen were expanded and therefore the damage degree increased. At 395.9 s,

the cracks in the middle part in the frontage of the specimen expanded and gradually cut through while the cracks at the bottom were staggered. The structure of the coal mass became increasingly unstable. At 396.9 s, the primary crack occurred in the specimen while the cracks in the middle part were totally connected. Moreover, the width and length of cracks in the lower part witnessed great increases and the cracks at the bottom were connected. Additionally, secondary cracks developed into secondarily primary cracks. The through-running cracks showed the combination of tensile and shear failure. Repetition

(4) Responses of EP signals

As shown in Figure 8, abundant EP signals can be generated during the damage of the gas-bearing coal under load. The changing trend of the EP was consistent with that of stress and there was a favorable corresponding relationship between EP and stress. With the increase of stress, damage in the specimen evolved. As a result, new fracturing constantly happened (shown as the growth of AE count and amplitude in Figure 6) and cracks constantly expanded (see Figure 7). During the above damage evolution, the EP intensity constantly rose. During the loading of the specimen, the EP intensity rose at a ladder type at 299.1 s and 359.6 s, with a significant increase amplitude. The phenomenon conformed to the time moments when stress and strain suddenly changed in Figure 5 and the time moments when AE count and amplitude varied suddenly in Figure 6. At these moments, the EP damage dramatically rose and therefore micro-cracks rapidly increased, showing growing strength. As a result, huge energy was released, which was also verified in Figure 7. At 396.9 s, as stress maximum appeared, the specimen was subjected to primary micro-cracks to thus be damaged due to loss of bearing capacity. In this case, the specimen was greatly and rapidly damaged. Moreover, the EP dramatically fluctuated and rapidly increased to a maximum, showing an extremely significant response. Afterward, the EP intensity rapidly reduced and stabilized at a low level. After the specimen was damaged, stress rapidly declined and the EP rapidly reduced and stabilized at a low level.
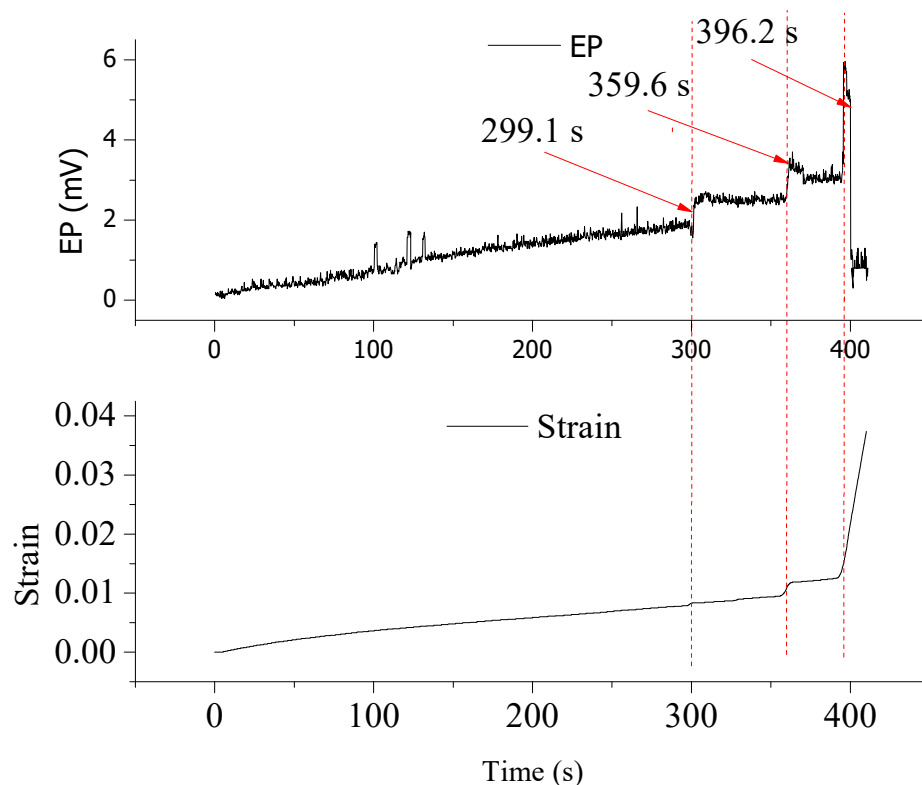

Figure 8. Curves of strain and EP with respect to loading time.

The strain's response characteristics were similar to the stress response. The difference was that the large stress drop occurring at 299.1 s. Currently, since the specimen was still in the elastic loading stage, the strain changes little even the EP response was significant. When loading phase of sample becomes to be plastic phase, especially around the failure, the strain response became more significant. It indicated that the strain monitoring is more sensitive when the specimen is plastic, especially for the main rupture.

The representative time points were selected to calculate corresponding LS levels. On this basis, the abnormal response characteristics of EP, AE, and crack expansion are attained, as shown in Table 2 and their datum statistics is displayed in Figure 9.

Table 2. Statistics on characteristics of EP, AE and crack expansion under different loading time moments (stress levels)

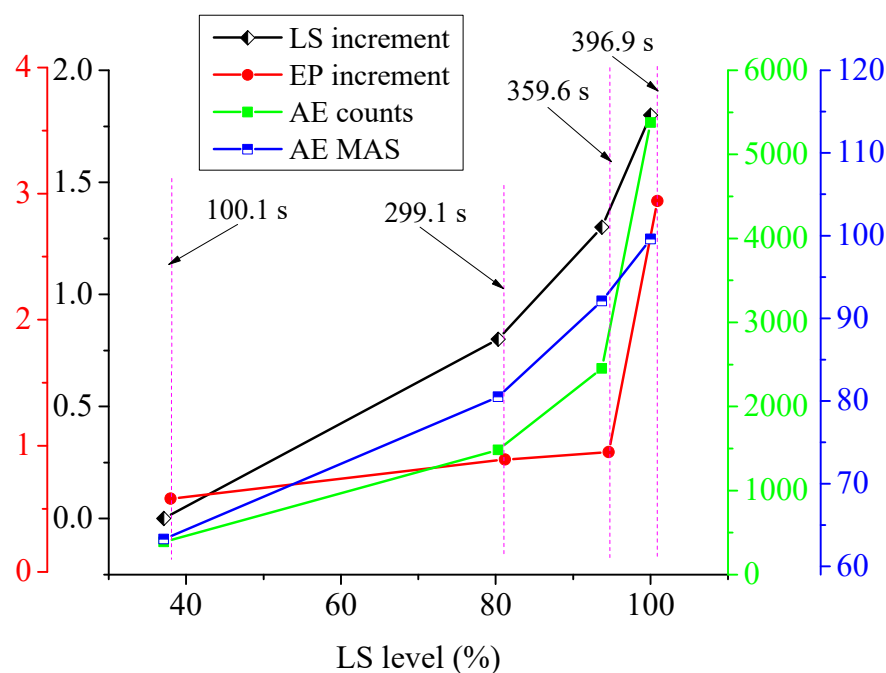| Time (s)	LS Level (%)	Stress Response	EP Response	Crack Expansion
100.1	37.1	Steady increase	Recover after the sudden change	No significant cracks
299.1	80.3	Recover after the sudden change	Rise after the sudden change	Two thin and long cracks
359.6	93.7	Recover after the sudden change	Rise after the sudden change	Cracks running from the top to the bottom
396.9	100	Cliff-type reduction	Sudden change to the maximum and then reduce	Increases in crack width and length

Figure 9. Datum statistics on EP and AE responses at different stress levels.

As shown in Table 2 and Figure 9, on the condition that stress suddenly changed, EP and AE tended to vary suddenly, showing significant abnormal response characteristics, and cracks greatly expanded and constantly aggravated. Correspondingly, the higher the stress level was and the larger the sudden change of stress was, the more significant the damage of the coal mass and thus the more dramatic the abnormal responses of EP and AE. It meant that the larger the increment of EP was, the more the AE counts and the higher the intensity. Additionally, crack expansion enhanced to thus aggravate the damage of the coal mass.

Therefore, based on the changes of stress and AE and analysis result of crack expansion, the change trend and response characteristics of EP can reflect the stress state of the specimen and reveal its damage-evolution process.

3.2. The EP Response Results under Different Gas Pressures

The EP responses under different gas pressures are shown in Figure 10. It is worth noting that gas pressure of 0 MPa means that gas is not injected into the cylinder and previous air in the cylinder is not extracted. Therefore, the air press is kept as the standard atmospheric pressure.
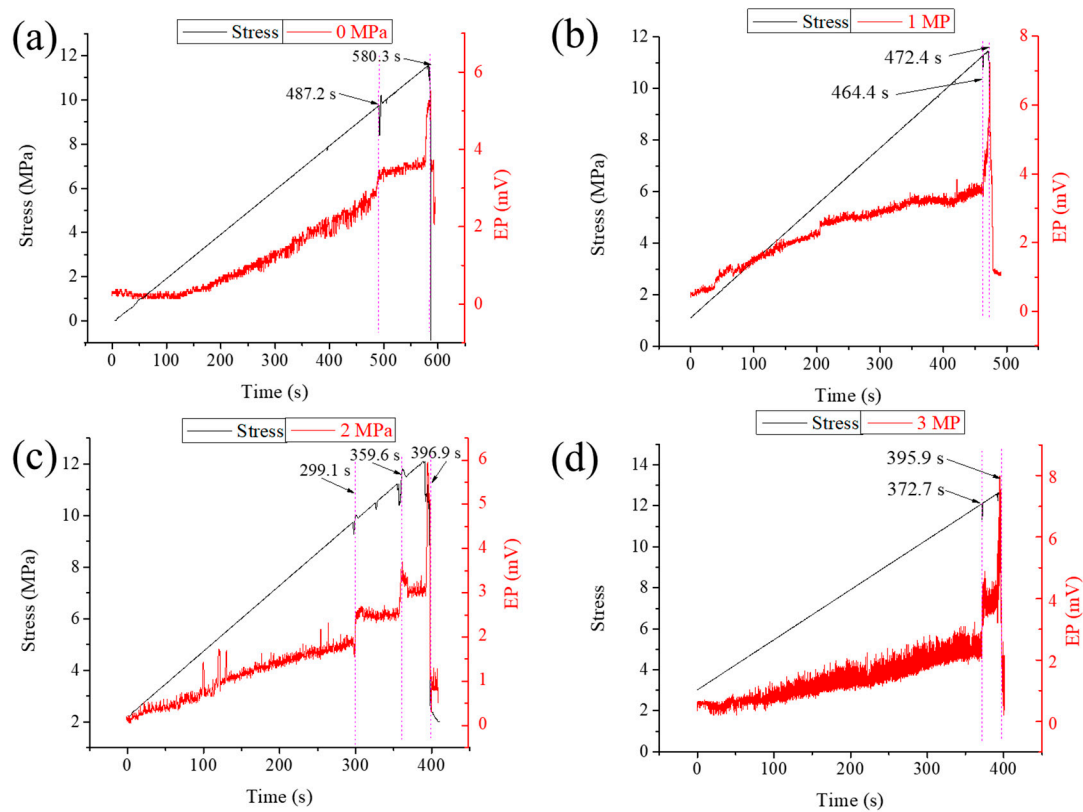

Figure 10. Changes of stress and EP during damage of coal mass under load under different gas pressures. Black and red actual lines represent the changes of stress and EP with loading time, respectively. (**a**) 0 MPa, (**b**) 1 MPa, (**c**) 2 MPa, (**d**) 3 MPa.

As shown in Figure 10, the EP responses under different gas pressures exhibited a basically same change law, which was similar to the results shown in Section 3.1 (4) With the increase of stress, the damage of the specimen under load constantly exacerbated and EP intensity gradually grew. When the specimen was subjected to a serious structural damage, stress suddenly changed and therefore the EP tended to vary abruptly (see 487.2 s in Figure 10a, 464.4 s in Figure 10b, 299.1 s and 359.6s in Figure 10c, and 372.7 s in Figure 10d). The specimen lost its bearing capacity after being subjected to primary crack and therefore stress declined at a cliff type and the EP also rapidly rose to the maximum, with the largest sudden change (see 580.3 s in Figure 10a, 472.4 s in Figure 10b, 396.9 s in Figure 10c, and 395.9 s in Figure 10d).

The broken strength, the strain maximum, the EP maximum, and the EP variation coefficient of specimens under different gas pressures were computed, as shown in Figure 11.
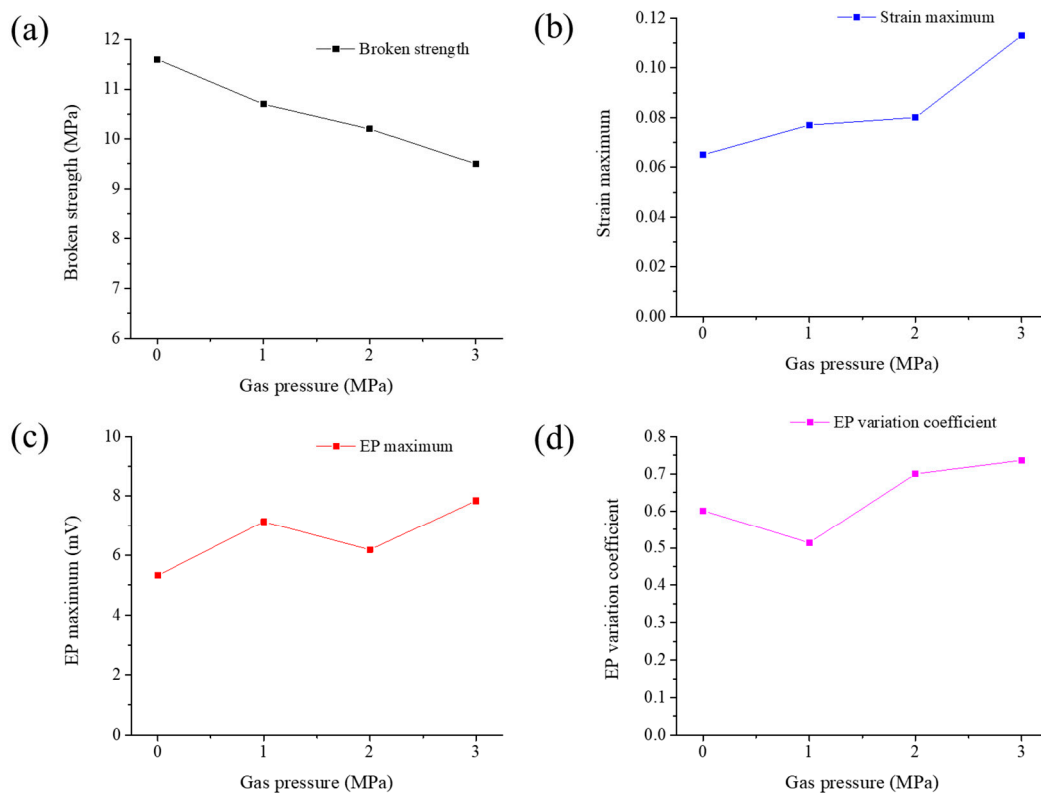
Figure 11. Statistical results of EP responses under different gas pressures. (**a**) Broken strength of specimen, (**b**) strain maximum of specimen, (**c**) EP maximum, (**d**) EP variation coefficient.

(1) The effective stress on the gas-bearing coal can be expressed as follows [34]:

$$\sigma_e = \sigma_L - \varnothing P - 2a\rho_s RT \ln(1 + bP)/3PV_m \tag{1}$$

where, σ_e, σ_L, $\varnothing$, P, a, ρ_s, R, T, b, and V_m refer to effective stress, LS, equivalent pore coefficient, gas pressure, ultimate gas adsorption of unit mass of rock mass at experimental temperature, apparent density of coal, molar gas constant, absolute temperature, adsorption constant, and molar volume, respectively.

Owing to the other conditions are unchanged, the aforementioned formula can be simplified if only the broken strengths (effective maximum stress on the specimen) of specimens under gas pressures were compared. It meant that relative broken strength ($\sigma_e\prime$) can be simplified and expressed by using the difference between LS maximum and gas pressure:

$$\sigma_e\prime = \sigma_t - P \tag{2}$$

As shown in Figure 11a, with the growth of gas pressure, the relative broken strength of the specimen gradually declined. Under the gas pressure of 3 MPa, the relative broken strength of the specimen significantly reduced, decreasing by 18.1% compared with that without gas pressure.

(2) The deformation of the specimen can be represented by using axial mean strain. As shown in Figure 11b, the deformation of the specimen greatly increased with increasing gas pressure. When the gas pressure was 3 MPa, the maximum strain rose by 112.3% compared with that on the condition of having no gas pressure.

(3) As shown in Figure 11c, the EP maximum tended to occur before or after primary micro-cracks of specimens, which was the most significant characteristic of the EP abnormal response. With the increase of gas pressure, although the EP maximum slightly fluctuated, it generally rose, implying that

gas pressure promoted the EP response and therefore EP maximum was at a high level, which was more valuable for analysis.

(4) The EP variation coefficient is the ratio of mean to standard deviation of whole EP data, which can objectively describe the fluctuating response of EP. As shown in Figure 11d, similar to the EP maximum, the EP variation coefficient also generally grew with the increase of gas pressure.

The aforementioned results showed that gas pressure promoted the EP response. The EP response characteristics can monitor the evolution process of damage and fracturing of gas-bearing coal (especially coal containing high content of gas).

4. Discussion

4.1. Damaging and Fracturing Process of Gas-Bearing Coal

The coal belongs to a typical heterogeneous structure, which contains a great number of micro-defects including pores, cracks, and dislocation, that is, Griffith defects [35]. The result can be clearly verified by observing the microstructures of gas-bearing coal by using the scanning electron microscope (SEM) (see Figure 12).
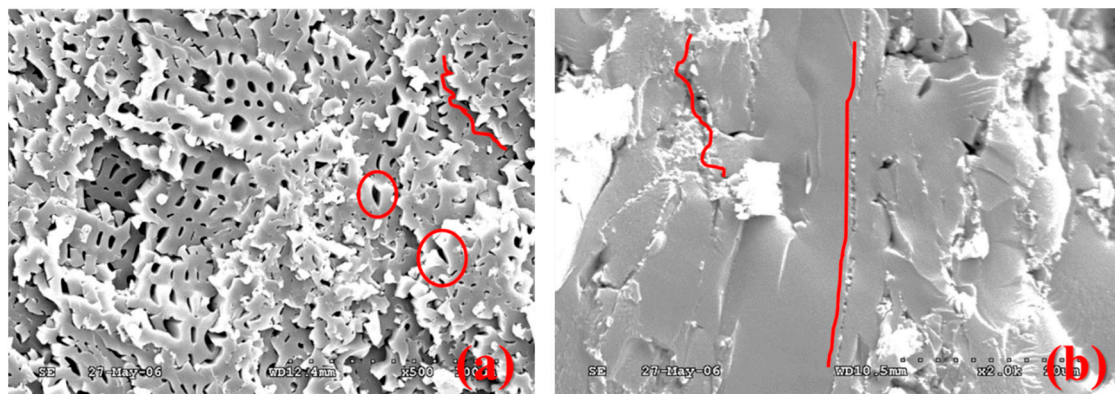

Figure 12. SEM images of microstructures of coal mass before loading. (**a**) Primary pores are abundant and crack was even, mostly appeared as spongy shape under magnification of 500 times; (**b**) Numerous cracks were found in pore clusters under magnification of 5000 times. Red curves refer to the tracks of cracks while red circles represent the location of cracks.

Cracks first initiated at the edge of primary cracks. After reaching the critical breaking strength, cracks expanded along a certain angle to thus generate new cracks. With the constant increase of stress, the damage of the coal mass exacerbated. Therefore, many micro-cracks appeared, expanded, split, closed and mutually connected along the direction with a weak strength to thus form a failure zone of cracks with a certain width. The phenomenon resulted in the generation of micro-cracks in the specimen finally (see Figure 7). Figure 13 displays the images of different fracture surfaces in the damaged gas-bearing coal at different magnification times. According to the pictures, the generation and expansion of cracks during the fracturing of coal as well as the inflection, bending, and splitting during the expansion can be clearly observed.
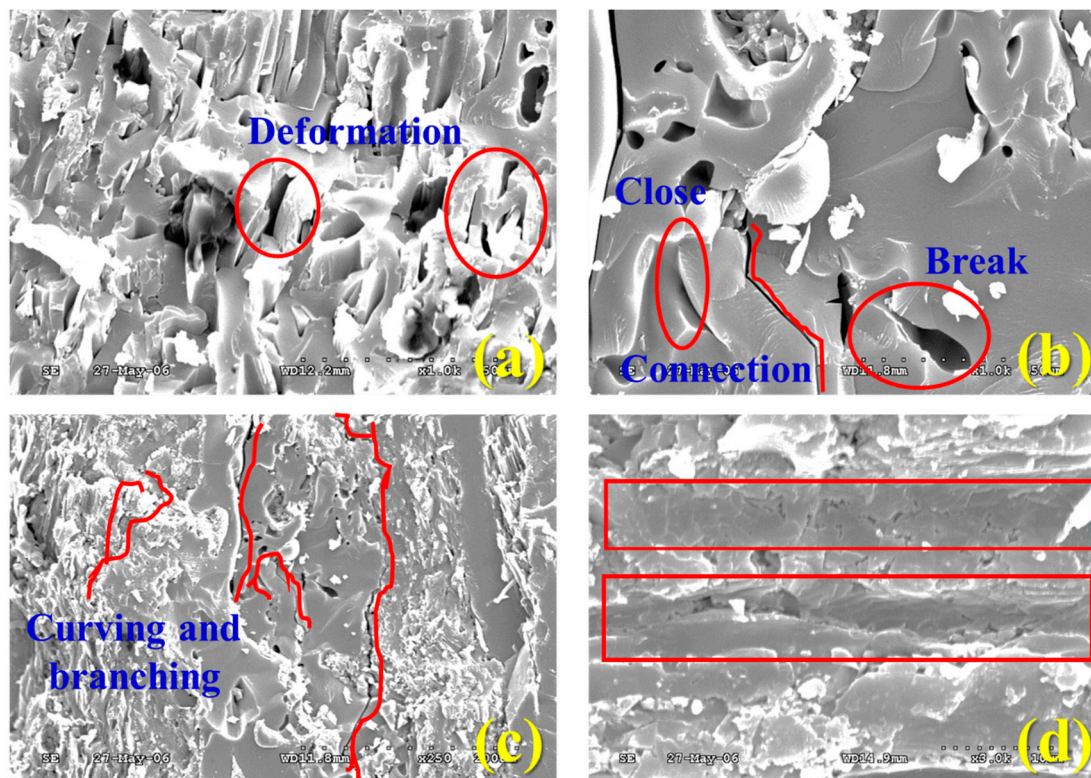
Figure 13. SEM images of microstructures of damaged gas-bearing coal; (**a**) Primary pores were deformed under magnification of 1000 times. (**b**) Pores were damaged, closed and then connected under magnification of 2000 times. (**c**) Tensile cracks were bent and split, which were densely distributed under magnification of 250 times. (**d**) Fracture surface appeared as step-shaped and river-shaped fractures under magnification of 100 times. Red rectangles denote the location of fractures.

4.2. The EP Response Analyses

As a micro-molecular mixture, coal is composed of multiple atom groups. The interiors of micro-molecules are connected through multiple bridge bonds, such as covalent bond, hydrogen bond and Van der Waals' force. The atom groups carry non-uniformly distributed charges so that they show polarity outward. As a result, the micro-surface of the rock mass shows weak electrical property [36] and the surface charge density exhibits the magnitude of 10^{-5}~10^{-4} C/m^2 [37], endowing the rock mass with a certain conductivity. Under the effect of external factors, the charged groups on the surface can lead to charge separation to form electric field. When the gas-bearing coal is damaged and deformed, the particles of coal matrix, mineral particles, and cement in internal structure of coal are subjected to relative slippage and dislocation to generate free charges due to the friction effect. The combined effect between triboelectrification and thermionic emission effect induces the EP response. However, the initiation and expansion of cracks can cause the fracturing of cementitious chemical bonds (even covalent bonds) between coal molecules to generate dangling bonds. It consequently leads to charge separation. Additionally, when stress is applied to micro-cracks, stress concentration effect occurs at the tip of cracks, which causes the energy in coal molecules to dramatically rise at the crack tip. Furthermore, molecular structures are subjected to distortion while outer electrons of molecules escape [16,19,24,26,28].

The charge separation and charge accumulation happening in the aforementioned process can lead to electrostatic charge field, which can be regarded as a point source of the surface EP effect. The interior of the coal mass is composed of heterogeneous coal matrixes and pores filled with gas molecules and coal matrix is greatly different from gas molecules in dielectric constant. Therefore, the polarization electric field can be formed at the interfaces of different dielectrics. Thus, it can be considered that EP

at a point within the coal mass is formed due to the superposition of constantly generated charges under the combined effect of variable static electric field and polarization electric field [38]. To simplify the solution process of EP, the EP value can be calculated with imaging method [39]. As shown in Figure 14, it is assumed that the dielectric constants of two semi-infinite dielectrics (coal matrix and gas) are ε_1 and ε_2 and their interface is set as M. Moreover, it is supposed that a point charge appears at a point O, with the electric charge quantity of q. Additionally, it is assumed that the symmetrical location of O in the mirror image corresponding to the interface M is $O\prime$, with the electric charge of $q\prime$.
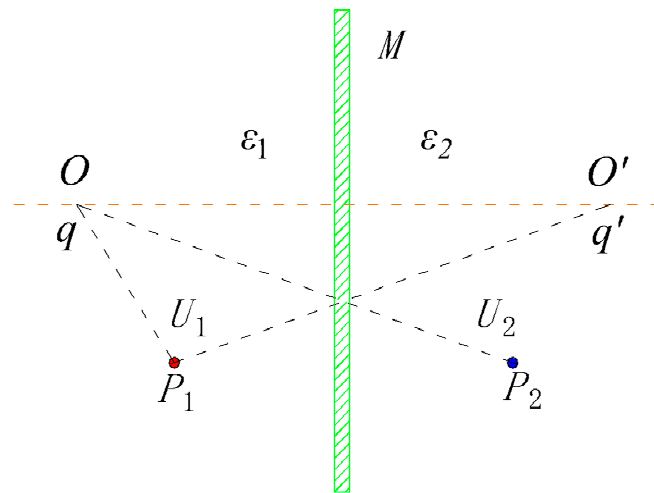

Figure 14. The sketch map of the imaging method for solving EP based on a single boundary. Where $O\prime$ and O refer to the true and imaging charges while U_1 and U_2 denote the EPs at points P_1 and P_2, respectively.

Therefore, the EP at the point P_1 with the same dielectric location with O is expressed as U_1. Similarly, the EP at the point P_2 with the same dielectric point with $O\prime$ is calculated as U_2. Thus,

$$U_1 = q(1/r + K_{12}/r_1)/(4\pi\varepsilon_1) \tag{3}$$

$$U_2 = q(1/r_2 - K_{12}/r_2)/(4\pi\varepsilon_2) \tag{4}$$

where, r, r_1, r_2, and $K_{12} = (\varepsilon_1 - \varepsilon_2)/(\varepsilon_1 + \varepsilon_2)$ refer to the distance of P_1 to point O, the distance of $O\prime$ to the point P_1, the distance of O to the point P_2, and the reflection coefficient of the dielectric ε_1 to ε_2, respectively.

The aforementioned model is popularized to the finite boundary. As shown in Figure 15, the point charge q is bounded within a finite space by four boundaries (A, B, C, and D) and isolated from different dielectrics of external environment. The initial imaging charges of q generated in the four boundaries are q_1, q_2, q_3, and q_4, respectively. Similarly, existing imaging charges can generate new imaging charges along the other boundaries. In this way, there are infinite such imaging charges. However, the farther the new imaging charges distancing to the point charge is, the less significant their effect on the EP of the measurement point [40].
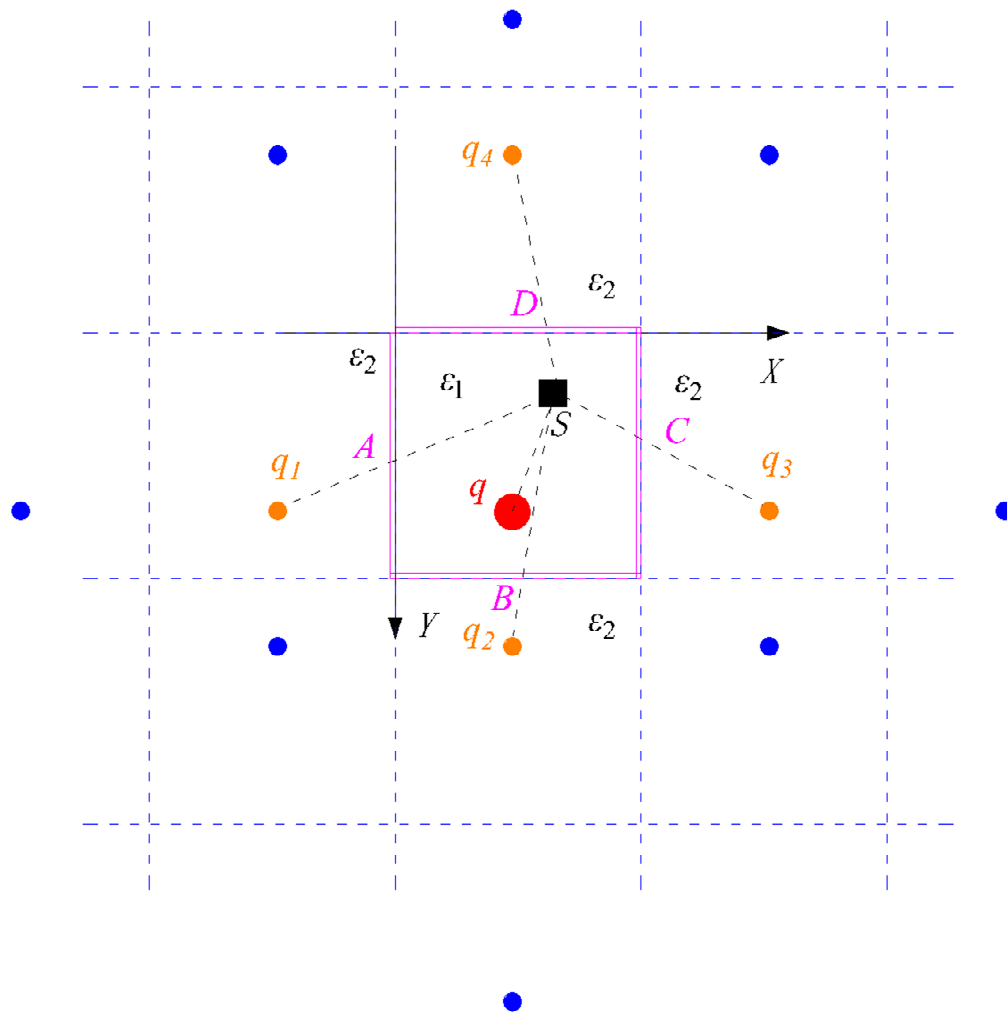
Figure 15. Schematic map of imaging method for solving EPs under finite boundaries. The red solid circle and the pink box refer to actual point charge and four boundaries, respectively. Brown solid circles denote the initial imaging charge of actual point charge at the aforementioned boundaries while blue solid circles represent new imaging charges generated based on the initial imaging charges at the corresponding boundaries. The solid box refers to the location of the point *S*.

Through simplification, the EP at the measurement point *S* can be expressed as follows:

$$U_S = q/(4\pi\varepsilon_1 r) + \sum_{j=0}^{m} K_{12}{}^j \sum_{i=0}^{n} K_{12}{}^i \left[1/r_{1ij} + 1/r_{2ij} + 1/r_{3ij} + 1/r_{4ij}\right] / (4\pi\varepsilon_2) \tag{5}$$

where, $K_{ab}{}^i$ and $K_{ab}{}^j$ separately denote reflection coefficients while *i* and *j*. are superscripts representing the reflecting interfaces separately parallel to axes *x* and *y*. Moreover, *n* and *m* denote corresponding mirror imaging reflections and r_{1ij}, r_{2ij}, r_{3ij}, and r_{4ij} refer to the distances of imaging charges to the measurement point *P*.

4.3. The Influence of Gas on EP Effect

As the pore structure is well developed in coal, a large amount of gas is adsorbed on the coal mass after the complete adsorption. Non-adsorbed gas freely moves in coal pores at a free state. A gas-solid coupling system is formed with the adsorbed and free-state gas with coal pores. The formation of the system changes the mechanical properties as well as the damage and fracturing process of the coal mass to thus further influence of response characteristics of EP [6].

(1) The influence of gas on mechanical properties of the coal mass

After gas is fully absorbed by the coal mass, surface free energy of pores reduces [41]. As a result, the attractive force between coal molecules on the fracture surface decreases and the capability of matrix for restricting coal molecules weakens, triggering the expansion-induced deformation of coal matrixes. Microscopically, the change is reflected by the reduced cohesion between coal matrix particles, which finally reduces the force and energy required during failure of the coal mass, and therefore the failure strength declines while the deformation amount increases. This has been verified in the results of Section 3.2, as shown in Figure 10a,b. Additionally, the free-state gas enters large microscopic fractures in the coal mass under the effect of pore pressure to therefore strengthen the effective normal stress, and the structure of fractures will be split and expanded. Additionally, the frictional resistance of cracked surfaces will also be weakened. Moreover, the pore structure is changed, and the mechanical strength of pore structures reduced [42].

(2) The influence of gas on the damage and fracturing process of the coal mass

The process of deformation and fracturing of the coal mass is discontinuous and non-uniform and sometimes local zone is subjected to expansion or shrinkage. On the one hand, gas can deteriorate the structure of the coal mass and promote the damage and fracturing of the coal mass. On the other hand, gas provides confining pressure to change the stress state of the interior of the specimen [42,43]. Under the effect of axial compression stress, the coal mass is subjectged to transverse deformation to induce transverse tensile stress. Under the effect of axial compression stress, transverse tensile stress, and transverse gas stress (confining pressure), the specimens are characterized by the combination of tensile and shear failure. Then the fracturing direction of the specimen shows a certain included angle with the axial direction. With the increase of gas pressure, the difference between confining pressure and peak loading stress leading to failure of the coal mass reduces, and such failure characteristic of the specimen becomes more significant, with a larger included angle (see Figure 16).
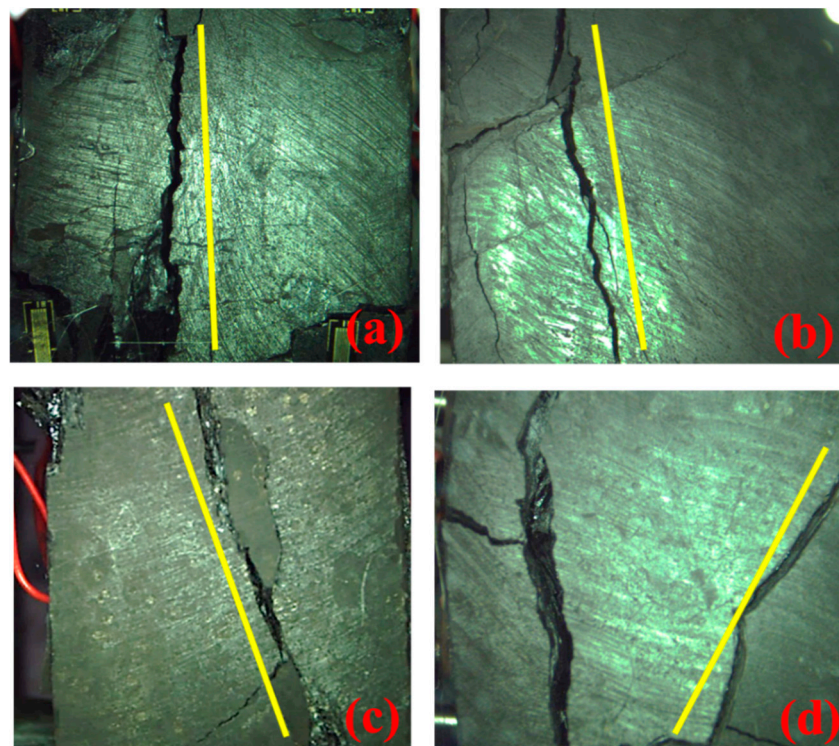

Figure 16. Pictures of real coal mass under load under different gas pressures. (**a**) 0 MPa, (**b**) 1 MPa, (**c**) 2 MPa, (**d**) 3 MPa.

(3) The influence of gas on the EP response

The presence of gas promoted the evolution of damage and fracturing of the coal mass. In particular, the expansion effect and the friction effect of cracks promoted the EP response. Additionally, free-state gas migrated and diffused in coal pores to constantly lead to collision and energy exchange with the edge of micro-cracks and to generate streaming EP with a certain intensity as well.

The EP response was triggered by cracks in the coal mass under load and abnormal sudden change of EP can reveal the failure of the coal mass. For this reason, during the fracturing of gas-bearing coal under load, with the increase of gas pressure, cracks were likely to initiate and propagate in the coal mass and friction effect was strengthened. As a result, the EP effect was more significant, and EP maximum and EP variation coefficient both gradually rose, which are also varied in Section 3.2, as shown in Figure 10c,d.

4.4. Analysis of the EP Response of Gas-Bearing Coal in Different Loading Stages

By taking 2.0 MPa of gas pressure as an example, the damage process of the gas-bearing coal under load can be approximately divided into five stages (see Figure 17) [32].
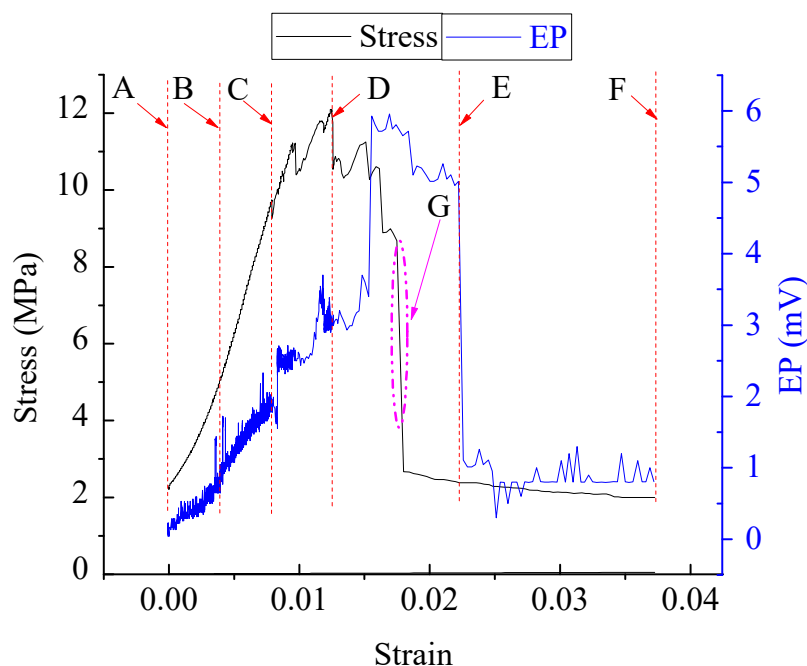

Figure 17. Complete stress-strain curves during the damage of gas-bearing coal under load.

(1) AB stage: Under the effect of stress, the original structural plane and micro-cracks were compacted and closed gradually. Therefore, the EP intensity in the initial stage was generally low while greatly fluctuated. In terms of the EP effect in the stage, the friction effect generated due to the closure of primary crack surfaces mainly appeared while new cracks hardly occurred.

(2) BC stage: In the elastic stage, the coal matrix was mainly subjected to linear-elastic deformation while suffered from little plastic damage. With the increase of strain, stress steadily rose and therefore new primary cracks constantly reached the critical strength, thereby causing the initiation, expansion, and splitting of cracks and steady rise of the EP intensity. In terms of the EP response in the stage, the friction effect between particles of coal matrix and crack surface and little crack expansion effect were mainly found. The presence of gas aggravated the damage and deformation of the coal mass, with a significant promotion effect on the EP response.

(3) CD stage: In the yielding stage, after stress reached the yield point, some irreversible deformations appeared in the specimen. Micro-cracks greatly expanded and resulting charge separation was taken as the dominant mechanism of the EP response. Moreover, the EP response was relatively active, and the EP intensity constantly rose.

(4) DE stage: Plastic deformation mainly happened in the stage. The damage of the specimen constantly exacerbated and micro-cracks and secondary cracks rapidly expanded and connected, which resulted in the occurrence of a primary crack. In the process, a great quantity of intermolecular and even intramolecular chemical bonds in the coal was fractured to thus further generate many charge separations. Additionally, the rapid expansion of cracks also led to the generation of friction effect and a great number of charges were accumulated under the two effects. Owing to the local zone was seriously damaged, the electron-escaping effect caused by stress concentration was also enhanced. The combined effect of multiple factors caused many charges to instantaneously accumulate. As a result, dramatic fluctuation appeared, and EP signals rapidly rose to a maximum. The promotion effect of gas was extremely significant (as shown in Figures 10 and 11).

(5) EF stage: Primary cracks appeared, and cracks fully connected, depriving bearing capacity of the specimen. After the specimen was completely damaged, generated friction effect, crack expansion, etc. of EP signals also basically ended. Therefore, the EP intensity also rapidly reduced and stabilized.

Combined with the analysis in Section 3.1., the EP response was closely related to loading state, AE response, and crack expansion, which can express the evolution of cracks and damage during the loading process of the gas-bearing coal. The presence of gas showed a promotion effect on the EP response. As shown in Figure 16, during DE stage, the specimen was greatly damaged and fractured and therefore failure happened to the coal. Moreover, the abnormal response of EP was extremely significant. The specimen was damaged, which meant that bearing capacity of the specimen rapidly reduced, that is, LS rapidly declined, which can be seen in G zone of Figure 17. In this case, EP rapidly rose to a maximum, which can be taken as the abnormal characteristic for the failure of the gas-bearing coal to monitor the failure of the coal mass.

4.5. Research Significance of the EP Effect of Gas-Bearing Coal

In the mining field of gas-bearing coal, dynamically monitoring the damage and fracturing process of gas-bearing coal is the premise of warning the coal and gas outburst disasters. In addition, EP monitoring can further reflect the stress level and damage state of the coal mass under different loading stages. Therefore, if the stress state of the coal mass cannot be tested directly, monitoring the EP response provides a favorable reference for monitoring the damage-evolution process of gas-bearing coal. Further investigating the EP effect and the mechanism of gas-bearing coal is conducive to further exploring the damage-evolution process of the coal mass. It is beneficial for the study on disaster-causing mechanism of coal failure under the stress-gas coupling effect. It also provides a new idea for monitoring the stability (nondestructive detection) of gas-bearing coal based on the EP response. Moreover, it provides a new idea for exploring the initiation and occurrence of rock and gas outburst disasters based on the EP response.

Compared with traditional geophysical information such as electromagnetic radiation and AE, the EP response is more accurate. Its monitoring process shows a low requirement for the shielding of environmental-noise and non-contact electromagnetic interference. Moreover, signal screening is not complex. Therefore, the EP response exhibits a favorable superiority in engineering application [26]. It possesses the important significance to be used to monitor the damage evolution of gas-bearing coal seams and provide an indication prior to forecasting dynamic disasters in mines.

5. Conclusions

During the loading and damaging process of gas-bearing coal, multi-information was measured and analyzed to obtain the research results as follow:

(1) Abundant EP signals are generated during the damage of gas-bearing coal under load. With the growth of stress, the damage of the specimen was aggravated, and EP was strengthened. Moreover, AE counts and amplitude increased, and crack expansion were exacerbated. When the specimen was subjected to local fracturing and stress suddenly changed, EP and AE tended to vary suddenly, and crack expansion was significant and constantly aggravated. The higher the stress level was and the greater the sudden change of stress was, the more dramatic the damage of the coal mass and therefore the greater the abnormal response of EP and AE. The EP response showed similar characteristics under different gas pressures and the presence of gas promoted the EP response. The changing trend and response characteristics of EP exhibit the stress state and reveal the damage-evolution process of the specimen.

(2) Under the coupling effect of stress and gas, the damage of the coal mass constantly aggravated. It caused internal cracks to constantly initiate, then propagate and finally converge, and connect, triggering the fracturing of the coal mass. Charge separation happened under the effects of crack expansion, friction effect between crack surface and coal matrixes, electron emission induced by stress concentration, etc. As a result, the EP response was triggered. Furthermore, the calculation method for EP is simplified with imaging method.

(3) After gas was fully absorbed by the coal mass, surface free energy of pores reduced, which caused the decline of intramolecular and intermolecular attractive forces. It led to expansion-induced deformation of coal and reduction of cohesion. This reduced the broken strength of the coal mass and increased deformation. Additionally, free-state gas entered large fractures in the coal mass under the effect of pore pressure. It had a splitting and expansion effect on fracture structure and weakened the friction resistance of crack surface. Therefore, the presence of gas promoted the crack expansion of the coal mass and friction effect to strengthen the EP effect. In addition, the electrokinetic effect generated due to the flow of free-state gas in pores also exerted a certain influence on the EP effect.

(4) At different loading stages, different factors dominated the EP response of gas-bearing coal. In the early stage of loading, the friction effect played a dominant part while crack expansion mainly appeared in the later period of loading. The electron emission was caused by stress concentration and the electrokinetic effect induced by gas flow both exhibited a certain effect during the whole loading stage. During the failure of the specimen, the EP rapidly rose to a maximum, so did the AE count. Moreover, signals showed a high amplitude and cracks rapidly expanded and ran through from the top to the bottom of the specimen. It led to the failure of gas-bearing coal finally. After the specimen was completely damaged, EP signals rapidly reduced and then stabilized. The abnormal characteristic of EP can be taken as an index for monitoring the stability of gas-bearing coal and warning the failure of the coal mass.

Author Contributions: Conceptualization and methodology: Z.L., E.W. and L.L.; analysis and investigation: Z.L. and Y.N.; original draft reparation, writing: Z.L. and Y.N.; review, editing and funding acquisition: Z.L., Y.N., E.W., L.L., H.W., A.M. and M. W.

Conflicts of Interest: The authors declare no conflict of interest.

Abbreviations

a	Ultimate gas adsorption	r_{3ij}	Distances of imaging charges to the measurement point P
b	Molar gas constant	r_{4ij}	Distances of imaging charges to the measurement point P
K_{12}	Reflection coefficient of the dielectric ε_1 To ε_2	T	Absolute temperature
$K_{ab}{}^{i}$	Reflection coefficients while i represent the superscripts of reflecting interface separately parallel to axes x and y	U_1	EP at the point P_1
$K_{ab}{}^{j}$	Reflection coefficients while j represent the superscripts of reflecting interface separately parallel to axes x and y	U_2	EP at the point P_1
m	Another corresponding times of mirror imaging reflection	U_S	EP at the measurement point S
n	Corresponding times of mirror imaging reflection	V_m	Molar volume
P	Gas pressure	ε_1	Semi-infinite dielectrics of coal
q	Charge quantity of initial charge	ε_2	Semi-infinite dielectrics of gas
R	Molar gas constant	$\varnothing$	Equivalent pore coefficient
r	Distance of P_1 To point O	ρ_s	Apparent density
r_1	Distance of $O\prime$ to the point P_1	σ_e	Effective stress
r_2	Distance of O to the point P_2	$\sigma_e\prime$	Relative broken strength
r_{1ij}	Distances of imaging charges to the measurement point P	σ_L	Loading stress
r_{2ij}	Distances of imaging charges to the measurement point P		

References

1. Song, X.; Li, X.; Li, Z.; Zhang, Z.; Cheng, F.; Chen, P.; Liu, Y. Study on the characteristics of coal rock electromagnetic radiation (EMR) and the main influencing factors. *J. Appl. Geophys.* **2018**, *148*, 216–225. [CrossRef]
2. Yuan, L. Theory and practice of integrated coal production and gas extraction. *Int. J. Coal Sci. Technol.* **2015**, *2*, 3–11. [CrossRef]
3. Lu, S.; Li, L.; Cheng, Y.; Sa, Z.; Zhang, Y.; Yang, N. Mechanical failure mechanisms and forms of normal and deformed coal combination containing gas: Model development and analysis. *Eng. Fail. Anal.* **2017**, *80*, 241–252. [CrossRef]
4. Ma, C.; Wang, P.; Jiang, L.; Wang, C. Deformation and Control Countermeasure of Surrounding Rocks for Water-Dripping Roadway Below a Contiguous Seam Goaf. *Processes* **2018**, *6*, 77. [CrossRef]
5. Hebblewhite, B.; Galvin, J. A review of the geomechanics aspects of a double fatality coal burst at Austar Colliery in NSW, Australia in April 2014. *Int. J. Min. Sci. Technol.* **2017**, *27*, 3–7. [CrossRef]
6. Tang, Z.; Yang, S.; Wu, G. Occurrence Mechanism and Risk Assessment of Dynamic of Coal and Rock Disasters in the Low-Temperature Oxidation Process of a Coal-Bed Methane Reservoir. *Energy Fuels* **2017**, *31*, 3602–3609. [CrossRef]
7. Freund, F.; Sornette, D. Electro-magnetic earthquake bursts and critical rupture of peroxy bond networks in rocks. *Tectonophysics* **2007**, *431*, 33–47. [CrossRef]
8. Marland, S.; Merchant, A.; Rowson, N. Dielectric properties of coal. *Fuel* **2001**, *80*, 1839–1849. [CrossRef]
9. Lamich, D.; Marschalko, M.; Yilmaz, I.; Bednářová, P.; Niemiec, D.; Kubečka, K.; Mikulenka, V. Subsidence measurements in roads and implementation in land use plan optimisation in areas affected by deep coal mining. *Environ. Earth Sci.* **2016**, *75*, 69. [CrossRef]

10. Lu, P.; Li, P.; Chen, J.; Zhang, C.; Xue, J.; Yu, T. Gas drainage from different mine areas: Optimal placement of drainage systems for deep coal seams with high gas emissions. *Int. J. Coal Sci. Technol.* **2015**, *2*, 84–90. [CrossRef]

11. Pillalamarry, M.; Harpalani, S.; Liu, S. Gas diffusion behavior of coal and its impact on production from coalbed methane reservoirs. *Int. J. Coal Geol.* **2011**, *86*, 342–348. [CrossRef]

12. Mishchuk, N.; Ralston, J.; Fornasiero, D. Influence of dissolved gas on van der Waals forces between bubbles and particles. *J. Phys. Chem. A* **2002**, *106*, 689–696. [CrossRef]

13. Karacan, C.; Okandan, E. Adsorption and gas transport in coal microstructure: Investigation and evaluation by quantitative X-ray CT imaging. *Fuel* **2001**, *80*, 509–520. [CrossRef]

14. Archer, J.; Dobbs, M.; Aydin, A.; Reeves, H.; Prance, R. Measurement and correlation of acoustic emissions and pressure stimulated voltages in rock using an electric potential sensor. *Int. J. Rock Mech. Min. Sci.* **2016**, *89*, 26–33. [CrossRef]

15. Steffanson, M.; Bone, D.J. Apparatus and Method for Electromagnetic Radiation Sensing. U.S. Patent 9,851,256, 26 December 2017.

16. Enomoto, Y.; Shimamoto, T.; Tsutumi, A. Rapid electric charge fluctuation prior to rock fracturing: Its potential use for an immedi-ate earthquake precursor. In *Proceedings of International Workshop on Electromagneticphenomenarelat to Earthquake Prediction*; Hayakawa, M., Fujinawa, Y., Eds.; Terra Scientific Publishing Co.: Tokyo, Japan, 1993; pp. 64–65.

17. Freund, F.T.; Takeuchi, A.; Lau, B.W. Electric currents streaming out of stressed igneous rocks—A step towards understanding pre-earthquake low frequency EM emissions. *Phys. Chem. Earth Parts A/B/C* **2006**, *31*, 389–396. [CrossRef]

18. Vallianatos, F.; Triantis, D.; Tzanis, A.; Anastasiadis, C.; Stavrakas, I. Electric earthquake precursors: From laboratory results to field observations. *Phys. Chem. Earth Parts A/B/C* **2004**, *29*, 339–351. [CrossRef]

19. He, X.; Nie, B.; Chen, W.; Wang, E.; Dou, L.; Wang, Y.; Liu, M.; Hani, M. Research progress on electromagnetic radiation in gas-containing coal and rock fracture and its applications. *Saf. Sci.* **2012**, *50*, 728–735. [CrossRef]

20. Wang, X.; Liu, X.; Wang, E.; Li, X.; Zhang, X.; Zhang, C.; Kong, B. Experimental research of the AE responses and fracture evolution characteristics for sand-paraffin similar material. *Constr. Build. Mater.* **2017**, *132*, 446–456. [CrossRef]

21. Yoshida, S.; Clint, O.C.; Sammonds, P.R. Electric potential changes prior to shear fracture in dry and saturated rocks. *Geophys. Res. Lett.* **1998**, *25*, 1577–1580. [CrossRef]

22. Takeuchi, A.; Lau, B.W.; Freund, F.T. Current and surface potential induced by stress-activated positive holes in igneous rocks. *Phys. Chem. Earth Parts A/B/C* **2006**, *31*, 240–247. [CrossRef]

23. Wang, E.; Li, Z.; Liu, Z.; Li, Y.; Song, X. An Experimental Study on Surface Electric Potential of Loaded Coal. *Chin. J. Geophys.* **2009**, *52*, 641–649. [CrossRef]

24. Wang, E.Y.; Liu, X.F.; Li, Z.H.; Liu, Z.; He, X.Q. *Application of Electromagnetic Radiation (EMR) Technology in Monitoring and Warning of Coal and Rock Dynamic Disasters*; Springer International Publishing: Berlin, Germany, 2014; p. 4.

25. Li, Z.H.; Wang, E.Y.; He, X.Q. *Study on Theory and Mechanism of Surface Potential during Coal Fracture*; China University of Mining and Technology Press: Xuzhou, China, 2013.

26. Niu, Y.; Li, Z.; Kong, B.; Wang, E.; Lou, Q.; Qiu, L.; Kong, X.; Wang, J.; Dong, M.; Li, B. Similar simulation study on the characteristics of the electric potential response to coal mining. *J. Geophys. Eng.* **2017**, *15*, 42. [CrossRef]

27. Stavrakas, I.; Anastasiadis, C.; Triantis, D.; Vallianatos, F. Piezo stimulated currents in marble specimen: Precursory and concurrent-with-failure signals. *Nat. Hazards Earth Syst. Sci.* **2003**, *3*, 243–247. [CrossRef]

28. Aydin, A.; Dobbs, M.R.; Reeves, H.J.; Kirkham, M.P.; Graham, C.C. *Stress Induced Electric Field Measurements of Different Rock Lithology Using the Electric Potential Sensor*; American Rock Mechanics Association: New York, NY, USA, 2013.

29. Haas, A.K.; Revil, A.; Karaoulis, M.; Frash, L.; Hampton, J.; Gutierrez, M.; Mooney, M. Electric potential source localization reveals a borehole leak during hydraulic fracturing. *Geophysics* **2013**, *78*, D93–D113. [CrossRef]

30. Cai, Y.; Liu, D.; Mathews, J.P.; Pan, Z.; Elsworth, D.; Yao, Y.; Li, J.; Guo, X. Permeability evolution in fractured coal—Combining triaxial confinement with X-ray computed tomography, acoustic emission and ultrasonic techniques. *Int. J. Coal Geol.* **2014**, *122*, 91–104. [CrossRef]

31. Hou, W. Identification of coal and gangue by feed-forward neural network based on data analysis. *Int. J. Coal Prep. Util.* **2019**, *39*, 33–43. [CrossRef]

32. Kong, X.; Wang, E.; Hu, S.; Li, Z.; Liu, X.; Fang, B.; Zhan, T. Critical slowing down on acoustic emission characteristics of coal containing methane. *J. Nat. Gas Sci. Eng.* **2015**, *24*, 156–165. [CrossRef]

33. Lomas, H.; Roest, R.; Wells, A.; Wu, H.; Jiang, Z.; Sakurovs, R.; Stuart, R.; North, L.; Thorley, T.; Mahoney, M.R. Estimating coke fracture toughness using acoustic emissions and changes in coefficient of friction during scratch testing. *Fuel* **2018**, *226*, 564–572. [CrossRef]

34. Yin, G.Z.; Wang, D.K.; Zhang, D.M.; Huang, G. Solid-gas coupling dynamic model and numerical simulation of coal containing gas. *Chin. J. Geotech. Eng.* **2008**, *30*, 1430–1436.

35. Polesek-Karczewska, S. Estimation of the structure-related share of radiation heat transfer in a carbonised packed coal bed. *Fuel* **2017**, *195*, 243–252. [CrossRef]

36. Dokukin, M.; Olac-Vaw, R.; Guz, N.; Mitin, V.; Sokolov, I. Addressable photocharging of single quantum dots assisted with atomic force microscopy probe. *Appl. Phys. Lett.* **2009**, *95*, 173105. [CrossRef]

37. He, X.; Liu, X.; Nie, B.; Song, D. FTIR and Raman spectroscopy characterization of functional groups in various rank coals. *Fuel* **2017**, *206*, 555–563. [CrossRef]

38. Revil, A.; Ehouarne, L.; Thyreault, E. Tomography of self-potential anomalies of electrochemical nature. *Geophys. Res. Lett.* **2001**, *28*, 4363–4366. [CrossRef]

39. Patella, D. Introduction to ground surface self-potential tomography. *Geophys. Prospect.* **1997**, *45*, 653–681. [CrossRef]

40. Long, H.L.; Hao, J.Q. The Theoretical and Experimental Research on Self-Potential Tomography. *Chin. J. Geophys.* **2005**, *48*, 1408–1415. [CrossRef]

41. He, X.; Wang, E.; Lin, H. Coal deformation and fracture mechanism under pore gas action. *J. China Univ. Min. Technol.* **1996**, *25*, 6–11.

42. Liu, X.; Wang, X.; Wang, E.; Kong, X.; Zhang, C.; Liu, S.; Zhao, E. Effects of gas pressure on bursting liability of coal under uniaxial conditions. *J. Nat. Gas Sci. Eng.* **2017**, *39*, 90–100. [CrossRef]

43. Su, F.; Itakura, K.; Deguchi, G.; Ohga, K. Monitoring of coal fracturing in underground coal gasification by acoustic emission techniques. *Appl. Energy* **2017**, *189*, 142–156. [CrossRef]